



Heterogeneous Ag and ZnO Based Photocatalytic For Waste Water Treatment Under Different Irradiation Conditions

Khaled Saoud^{1*}, Rola Al Soubaihi¹, Shaukat Saeed², Nasr Bensalah³,
Mohamed Al-Fandi⁴, Tejvir Singh⁵

1. Liberal Arts and Science Program, Virginia Commonwealth University-Qatar, Doha, Qatar

2. Department of Metallurgy and Materials Engineering, Pakistan Institute of Engineering and Applied Sciences (PIEAS), Islamabad-45650, Pakistan

3. Department of Chemistry, Qatar University, Doha, Qatar

4. Nanotechnology Institute, Jordan University of Science and Technology Irbid, Jordan

5. Hamad Bin Khalifa University-Qatar, Doha, Qatar

Received 22 May 2017,
Revised 24 Sep 2017,
Accepted 29 Sep 2017

Keywords

- ✓ Photocatalysis;
- ✓ UV and Visible Light Photocatalyst;
- ✓ Degradation;
- ✓ Methylene Blue (MB);
- ✓ Ag/ZnO

s2kmsaou@vcu.edu
+97466037810
Fax: +21329824945

Abstract

Recently, we reported the synthesis of highly crystalline Ag (Silver) spheres on ZnO nanorods using Microwave Assisted Deposition-Precipitation (MADP) method with enhanced photocatalytic activity under visible light. In this paper, we report a comparative and experimental evidence for the potential applications of Ag/ZnO nanocomposites in waste water treatment. This paper presents the kinetics of Ag/ZnO toward Methylene Blue (MB) degradation under UV and Visible light irradiation, and the antibacterial properties toward Escherichia coli (E. coli) bacteria under light and in the dark. Results indicate that the presence of silver nanoparticles on the surface of ZnO leads to a significant and simultaneous enhancement of the optical and photocatalytic degradation efficiency of Ag/ZnO photocatalyst under UV and visible light irradiation, and was found to cause the inactivation of Escherichia coli (E. coli) bacteria under visible light and dark. These results suggest that the presence of Ag nanoparticles play a significant role in the photocatalytic activity and in the enhancement of the antibacterial activity towards inactivation of Escherichia coli (E. coli) bacteria.

1. Introduction

Recently, there has been an increasing demand on clean pollution free water resources. Most of the drinking water resources are contaminated with several toxic dyes such as methylene blue, and other phenols and phenolic and pathogenic microorganisms [1].

Recent studies reported the use of Nanophase semiconductor photocatalysts such as TiO₂ and ZnO that have novel and superior photocatalytic activity, availability, stability, low cost, and strong oxidative capacity [2, 3], when compared to the conventional methods used in dyes degradation and wastewater treatment [4]. In particular, ZnO nanoparticles show high photocatalytic activity due to their wide bandgap, high excitation binding energy, electron storage properties and have been used in many applications [5-10] and the ability to absorb a larger fraction of the UV light compared to TiO₂ [11]. However, ZnO has some limitations such as a rapid electron-hole recombination rate and limited activity under visible light [12]. Many studies reported the extending of ZnO absorption to the visible light by preventing electron-hole recombination through modifying the electronic structure of ZnO nanoparticles by doping ZnO with cationic or anionic or adding metals or non-metals [13-18]. It was reported that doping ZnO with noble metals leads to the creation of a local electric field and the optical vibration of surface plasmon especially in silver or gold that can induce enhancement in this electric field and hence enhance the photocatalytic activity [14, 19-21].

Silver nanoparticles gain a lot of interest in the recent years due to their thermal, biological, optical, photocatalytic and electrical properties which make it an excellent material for many applications such as sensor materials, electronic, solar, and cosmetic products, and anti-bacterial agents [22-30]. Silver ions

can exert strong inhibitory and bactericidal effects and have been used as an active agent for antimicrobial activities [27] by causing the release of K^+ ions from bacteria and attacking the enzymes and DNA in the bacterial cells [28]. Although there are numerous reports about the synthesis of Ag/ZnO and antibacterial activity using various synthetic routes and conditions [31-42], most of these reports focus only on the effect of the use of silver to enhance the absorption in the visible region due to its plasmonic effect.

The research conducted gave the conclusion; there are few detailed studies that focus on the effect of silver in the modification of ZnO photocatalyst and its role in enhancing the photocatalytic activity, kinetics, and antibacterial activity of ZnO photocatalyst under both visible lights, UV light, and in the dark irradiation conditions.

In the present context, we report a detailed study of the role of Ag in the photocatalytic, kinetics, and antibacterial activities of a heterogeneous Ag/ZnO photocatalyst by evaluating the property and photocatalytic performance of the ZnO as a result of silver addition as a potential photocatalyst for waste water treatment. The Ag/ZnO photocatalyst was prepared using Microwave Assisted Deposition- Precipitation method reported recently by our group [41] and its photocatalytic activities were compared to ZnO photocatalyst under UV, Visible Light, and in dark conditions.

2. Material and Methods

2.1 Synthesis of ZnO and Ag/ZnO Nanocomposites

All chemicals like such as Zinc Nitrate ($Zn(NO_3)_2$; Alfa Aesar), Silver Nitrates ($AgNO_3$; Sigma-Aldrich), Sodium Hydroxide (NaOH) (Alfa Aesar), and Glucose ($C_6H_{12}O_6$; Natural) were used as received without further purification. Distilled water was used in all the preparation. The synthesis procedure was reported in our previous paper [41]. In a typical synthesis process of ZnO nanorods, the precursor solution of zinc was prepared by dissolving 5 g of $Zn(NO_3)_2$ in 100 mL of ethanol in a 250 ml reaction flask. The solution was kept stirring while 1M NaOH was added dropwise to the solution until pH of the resulting solution reaches 10. The solution was subsequently placed in a microwave chemical reactor (MCR-3) where the microwave power was adjusted to 1/3 of full 800 W power rating. The solution remained exposed to microwave for approximately 10-15 minutes with 1 minute on and one minute off and was removed upon reaching the boiling point. The resulting solution was left to cool down naturally in the atmosphere. Finally, the precipitated particles were then filtered and collected after washing thoroughly several times with distilled water and ethanol. For the synthesis of Ag/ZnO with one wt. %, Ag nanoparticles (NPs) grown on the surface of the ZnO photocatalyst using Deposition Precipitation method (DP) by dissolving 4 g of as-prepared ZnO nanoparticles in 100 mL aqueous solution containing two wt. % of reducing agent (glucose) followed by vigorous stirring. Then, a proper amount (1 wt. % Ag) of Silver nitrates solution was added to the stirring solution dropwise until a pH value of 7 was obtained. Finally, the solution was placed in a microwave oven and irradiated for 10 minutes and was removed before reaching the boiling. The obtained solution was left to cool down naturally in the atmosphere, centrifuged at 5000 rpm for 5 minutes and the particles were collected and washed thoroughly with distilled water and ethanol.

2.2 Morphology and crystal structure of ZnO and Ag/ZnO Nanocomposites

2.2.1 Surface Area and X-Ray Diffraction (XRD)

All chemicals like such as Zinc Nitrate ($Zn(NO_3)_2$; Alfa Aesar), Silver Nitrates ($AgNO_3$; Sigma-Aldrich), Sodium Hydroxide (NaOH) (Alfa Aesar), and Glucose ($C_6H_{12}O_6$; Natural) were used as received without further purification. Distilled water was used in all the preparation. The synthesis procedure was reported in our previous paper [41]. In a typical synthesis process of ZnO nanorods, the precursor solution of zinc was prepared by dissolving 5 g of $Zn(NO_3)_2$ in 100 mL of ethanol in a 250 ml reaction flask. The solution was kept stirring while 1M NaOH was added dropwise to the solution until pH of the resulting solution reaches 10. The solution was subsequently placed in a microwave chemical reactor (MCR-3) where the microwave power was adjusted to 1/3 of full 800 W power rating. The solution remained exposed to microwave for approximately 10-15 minutes with 1 minute on and one minute off and was removed upon reaching the boiling point. The resulting solution was left to cool down naturally in the atmosphere. Finally, the precipitated particles were then filtered and collected after washing thoroughly several times with distilled water and ethanol. For the synthesis of Ag/ZnO with one wt. %, Ag nanoparticles (NPs) grown on the surface of the ZnO photocatalyst using Deposition Precipitation method (DP) by dissolving 4 g of as-prepared ZnO nanoparticles in 100 mL aqueous solution containing two wt. % of reducing agent (glucose) followed by vigorous stirring. Then, a proper amount (1 wt. % Ag) of Silver nitrates solution was added to the stirring solution dropwise until a pH value of 7 was obtained. Finally, the solution was placed in a microwave oven and irradiated for 10 minutes and was removed

before reaching the boiling. The obtained solution was left to cool down naturally in the atmosphere, centrifuged at 5000 rpm for 5 minutes and the particles were collected and washed thoroughly with distilled water and ethanol.

2.2 Morphology and crystal structure of ZnO-Ag/ZnO Nanocomposites

2.2.1 Surface Area and X-Ray Diffraction (XRD)

The surface area of ZnONanorods (NR) was found to be 5.305 m²/g, whereas surface area for Ag/ZnO was slightly less than the surface area of ZnONanorods and found to be 4.806 m²/g, which may be attributed to agglomeration of the nanoparticles upon Ag incorporation.

The structure and morphology of ZnO and Ag/ZnO have been confirmed studied using X-Ray Diffraction (XRD). High-Resolution Transmission Electron Microscopy (TEM), Specific surface area (SSA), and UV/Vis absorption spectra were also used for the characterization. The X-ray diffraction (XRD) of ZnO and Ag/ZnO nanoparticles samples were recorded by using a Rigaku MiniFlex600 (Cu K α radiation, λ wavelength =1.54 Å) XRD diffractometer. The surface area of ZnONanorods (NR) was found to be 5.305 m²/g, whereas surface area for Ag/ZnO was slightly less than the surface area of ZnONanorods and found to be 4.806 m²/g which may be attributed to agglomeration of the nanoparticles upon Ag incorporation. Figure 1 shows the XRD patterns of ZnO and Ag/ZnO nanoparticles with their respective Miller indices. The XRD patterns indicate that ZnO nanoparticles have a hexagonal crystal structure, exhibiting maximum diffraction from (101) crystal plane and Ag (111) crystal plane small peak can be observed at 37.9 which correspond to, respectively, confirming the presence of Ag in the sample. The ZnO peaks appear in the pattern of Ag/ZnO is similar to the peaks observed in pure ZnO, which indicates that there are no structural changes due to the addition of silver. Also, the pattern shows a peak at a 2 θ angle of 38.45°, which is due to the presence of (111) crystal plane of a silver particle on ZnO surface, was an excellent confirmation of formation of silver at ZnO. A detailed explanation of XRD pattern was reported in our recent paper [41].

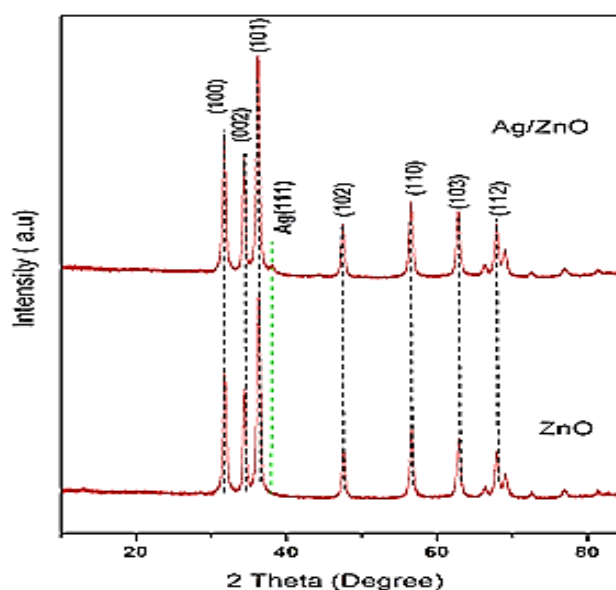


Figure 1: XRD patterns of ZnO and Ag-ZnO nanoparticles.

2.2.2 Energy dispersed X-Ray (EDX)

The chemical composition of Ag/ZnO nanocomposites was performed using scanning electron microscope (SEM)-Energy Dispersed X-Ray (EDX) with beam acceleration of 10 kV voltages. Figure 2 shows energy dispersed x-Ray (EDX) spectrum. The EDX spectrum confirms the presence of O, Zn, and Ag elements. These results also are a good agreement with the XRD results which confirmed that the sample composition consists of approximately 1% Ag and 99% ZnO.

2.2.3 Transmission electron microscopy (TEM)

Transmission electron microscopy (TEM; model: JEOL JEM-2100F) was used for the morphological characterization of the nanoparticles. Transmission Electron Micrographs (TEM) of ZnO and Ag/ZnO nanoparticles samples are shown in Fig. 3(a) and (b). It is evident from the micrograph that spherical Ag

nanoparticles (ranging from 5-60 nm) are dispersed on the surface of the ZnO nanorods (with diameters ranging from 10 to 20 nm).

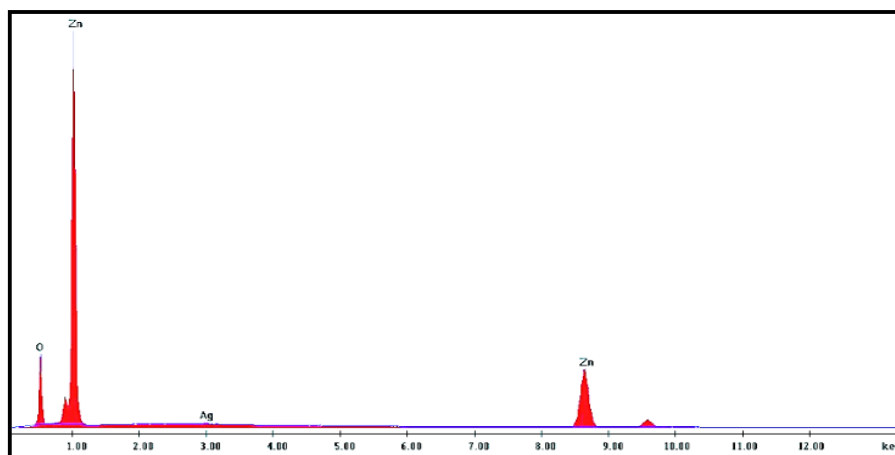


Figure 2: Energy dispersed x-Ray (EDX) of Ag/ZnO photocatalyst.

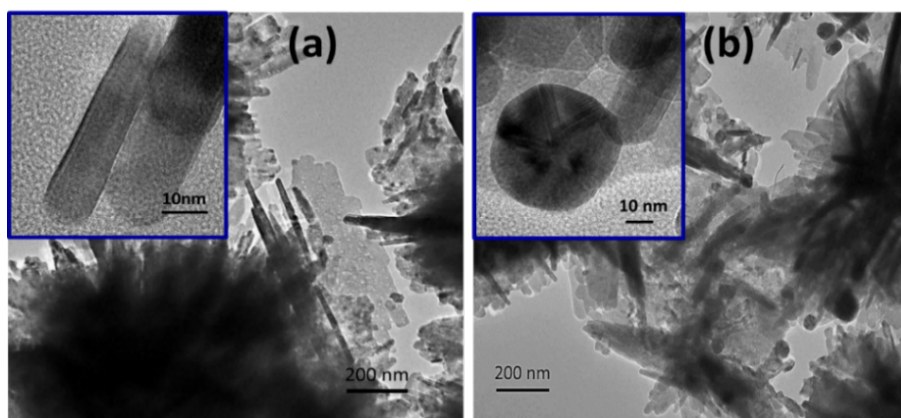


Figure 3: HRTEM micrographs of (a) as-prepared ZnO nanorods of diameter approximately 20 nm (b) Ag/ZnO nanocomposites showing the spherical Ag Nanoparticles (NP) with an approximately 40 nm in size on the surface of small ZnO nanorods (NR) of diameter approximately 20 nm.

2.2.4 UV/Vis absorption spectra of ZnO and Ag/ZnO Nanocomposites

UV/Vis absorption spectra of the nanoparticles were taken collected using UV1810 Series UV-Visible Spectrophotometer, Shanghai Yoke Instrument Co., Ltd. Figure 4 shows the UV/Vis absorption spectra of the ZnO and Ag/ZnO Nanocomposites.

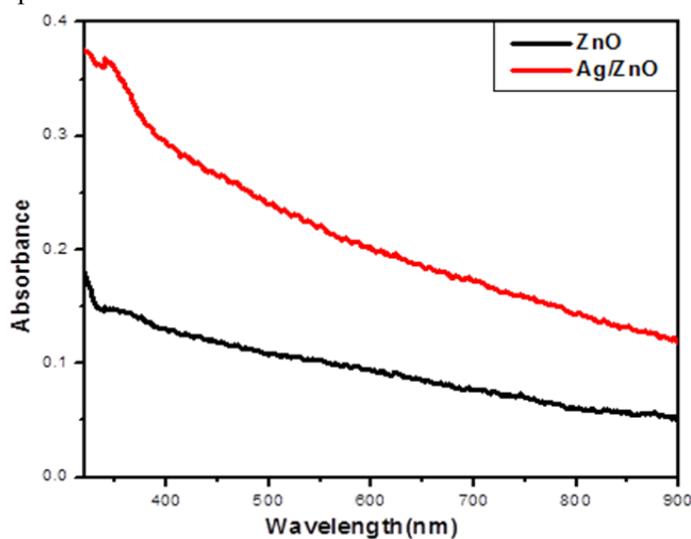


Figure 4: UV/Vis absorption spectra of ZnO and Ag/ZnO nanoparticles.

Both samples showed a strong absorption in UV region with an absorption onset at 400 nm. However, in the case of Ag/ZnO nanoparticles, we observed an enhancement of absorption spectra in both UV and visible region. The enhanced absorption is attributed to the interaction and the transfer of electrons between the silver and ZnO and the “Surface Plasmon Resonance (SPR)” absorption of silver nanoparticles. Even though the concentration of Ag nanoparticles is very low as observed in the TEM, EDX and XRD results, the SPR peak corresponding to Ag nanoparticles could not be clearly observed in the absorption spectra of the Ag/ZnO nanoparticles. The contribution of plasmonic absorption from Ag nanoparticles can be clearly observed as an increment in the optical absorption of the Ag/ZnO nanoparticles in the near UV/visible region. Similar results reported previously showed the improvement in the absorption near UV/visible region for Ag/ZnO nanoparticles [43-45]. A detailed characterization of Ag/ZnO nanocomposites including infrared and photoluminesces was reported in an earlier paper[41].

3. Results and discussion

3.1 Comparison between Photocatalytic degradation of MB on ZnO and Ag/ZnONanocomposites under UV and Visible light irradiation.

The photocatalytic degradation of MB under UV and Visible light irradiation using Ag/ZnONanocomposites as a photocatalyst was investigated and compared to ZnONanorods. Photocatalytic efficiency of the ZnO and Ag/ZnO was measured by degradation of Methylene Blue (MB). In a typical experiment, 5 mg/L of Methylene Blue (MB), as a representative dye indicator with natural pH of 5.8 at room temperature (23-25 °C) using UV-L (254 nm) at 15 W power rating and simulated solar light (AM 1.5G) with 1000 W/m² with 30 cm distance between the light source and the solution. A solution containing different concentrations of ZnO or Ag/ZnO was dispersed in 100 mL of a standard aqueous MB solution (20 mg/L) and stirred for one hour followed by withdrawing a certain volume of the suspension and finally, removing the photocatalyst by centrifuging. The photocatalytic degradation course of MB was then carried out for 2 hours and the photocatalytic reduction of MB concentration as a function of time was measured and recorded by measuring the optical absorption of the MB solution at 664 nm which correspond to the maximum absorption wavelength of MB using UV-Vis absorption spectroscopy to evaluate the photocatalytic degradation of MB. The MB solution with different doses of photocatalysts was kept in the dark for 30 minutes before the light irradiation to ensure that the adsorption-desorption equilibrium between the MB molecules and catalyst surface is reached.

The effect of the amount of ZnO and Ag/ZnO on the photodegradation efficiency of MB was investigated. Figure 5 represents the course of UV light and visible light normalised photocatalytic degradation of MB with (0.1 g/L figure 5(a) and 0.2 g/L figure. 5 (b)) of ZnO and Ag/ZnO photocatalysts. In the case of control (UV light only and no photocatalyst), the photocatalytic degradation of MB was less than 5% reduction in MB concentration after 2 hours of continuous UV light irradiation. While in the presence of ZnO photocatalyst, photocatalytic degradation of MB was observed with a significantly faster rate showing almost a 50% reduction in MB concentration at 0.1g/L and almost 70% under UV at 0.2 g/L after two hours of continuous radiation.

The rate of MB degradation under UV and visible light become faster upon using 0.1g/L of Ag/ZnO photocatalyst showing almost 87% reduction in 2 hours and reach nearly 94% under UV light and 98% under visible light irradiation using 0.2g/L of Ag/ZnO photocatalyst. It is important to mention that the degradation curve of Ag/ZnO nanocomposites under UV and visible light is not following the same curve, especially at times less than 90 minutes. The effect of Ag/ZnO nanocomposites with different photocatalyst doses on MB degradation has been investigated under both UV as well as visible light irradiation. Figure 6 shows the course of UV light and visible light normalised photocatalytic degradation of MB with different photocatalyst doses (from 0.1 to 1 g/L). It is important to mention that from (7% and reach 25% at 1 L/g dose) of MB is adsorbed on the catalyst before turning the Light on in the Visible photocatalytic degradation experiment.

It can be observed that the MB degradation under UV light proceeds faster than the MB degradation under visible light irradiation where a full reduction of MB at 1g/L of Ag/ZnO photocatalyst dose using UV light irradiation is reached in almost 37 minutes, while it reaches a full degradation under visible light in approximately 90 minutes. Our results agree with the results obtained by Seo et al.[46] where he explained the enhancements in the photocatalytic activity is mainly attributed to the decrease in the energy band gap of Ag/ZnO nanocomposites and the formation of Schottky barriers in the regions between Ag nanospheres and ZnONanorods as reported by Hairui Liu et al.[47] which leads to significantly improved photocatalytic activities under ultraviolet irradiation as a result of silver attachment.

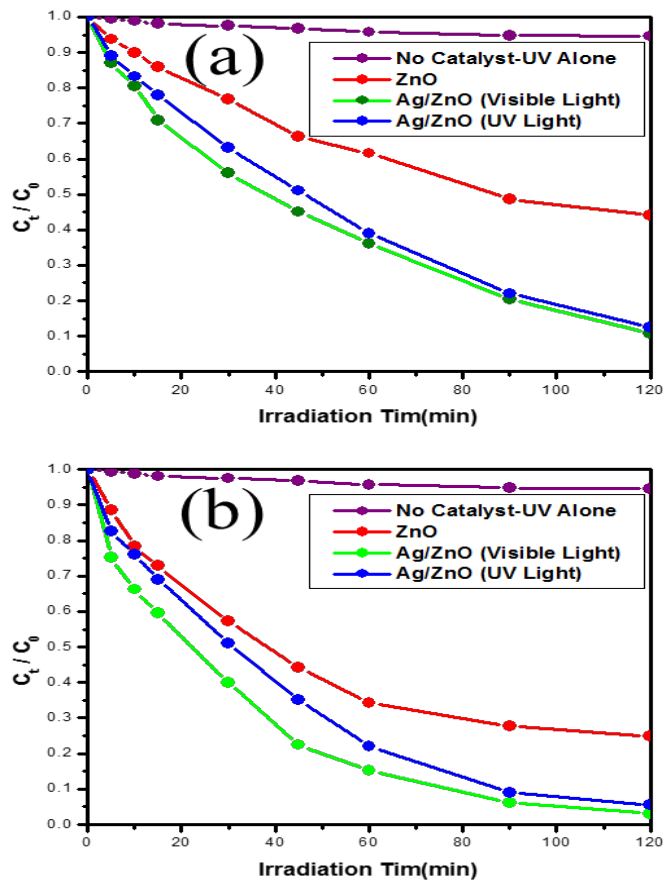


Figure 5: Comparison between Photocatalytic degradation of MB by ZnO and Ag/ZnO nanoparticles as a function of irradiation time at different Photocatalyst doses with a) 0.1 g/L photocatalyst dose b) 0.2 g/L photocatalyst dose. Reaction conditions: UV (UV-L (254 nm), 15 w) and visible light irradiation: 1000 W, 5 mg/L MB, natural pH 5.8, room temperature (23-25 °C).

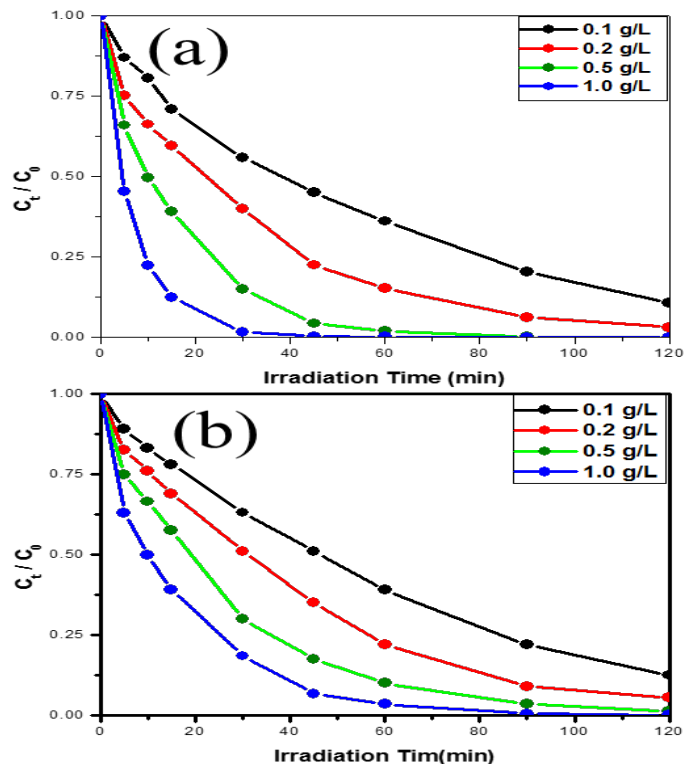


Figure 6: Degradation of MB as a function of irradiation time for different photocatalyst doses under a) UV light. b) Visible Light. Reaction conditions: UV (UV-L (254 nm)), 15 w) and visible light irradiation: 1000 W, 5 mg/L MB, natural pH 5.8, room temperature (23-25 °C).

While, in the case of the MB degradation under visible light, the enhanced photocatalytic activity of Ag/ZnO is mainly due to the interaction between Ag nanospheres and ZnO nanorods and strong localized "Surface Plasmon Resonance (SPR)" where electron transfers from Plasmon excited metallic Ag nanospheres to ZnO nanorods which effectively reduce the recombination between electron and hole pairs and increase lifetime of the electron–holes pairs and hence enhance the degradation efficiency.

We observed that the MB degradation on Ag/ZnO with doses (from 0.1 to 1 g/L) under UV and visible light is increased as the dose increased. In order to confirm these results, we measured the reaction rate constants of MB degradation reaction under UV and visible light irradiation conditions.

3.2 Kinetics of MB degradation on Ag/ZnO Nanocomposites under UV and visible light irradiation

The rate of MB degradation using Ag/ZnO nanocomposites under UV and visible light irradiation was investigated as a function of photocatalyst dose. We find that the degradation reaction is increased as the dose increased and reached complete reduction at 1g/L of Ag/ZnO photocatalyst in less than 37 minutes under UV irradiation and almost 90 minutes under visible light irradiation. However, at low doses, the degradation was less and never reached a complete reduction in 2 hours under both irradiation conditions. The degradation using 0.1g/L of Ag/ZnO photocatalyst was almost 87% under UV light, and 72% under visible light after 2 hours of continuous irradiation, and further increased to reach 98% under UV light and 80% under visible light at 0.2 g/L dose. Complete degradation was observed at 0.5 g/L dose after almost 60 minutes under UV light and 120 minutes under visible light irradiation as shown in figure 7a) and 7b).

Even though, the photocatalytic process using Ag/ZnO under UV and visible light irradiation leads to complete reduction of MB at doses higher than 0.5 g/L within less than 120 minutes, doses less than 0.5 g/L did not lead to complete degradation, high MB degradation percentage can be achieved within 120 minutes. The amounts of MB that remain in solution are still with the contaminant levels regulated by environmental agencies. These results indicate that increasing the doses of Ag/ZnO photocatalyst result in increasing the MB photodegradation efficiency under UV and visible light irradiation conditions. We attributed these results to the synergetic effect between Ag and ZnO and availability of the active sites on the catalyst surface and the penetration of UV light into the catalyst suspension where total active surface area increases with increasing catalyst dosage [48] as shown in figure 6.

To study the kinetics of the MB degradation using Ag/ZnO photocatalyst under UV or visible light irradiation, According to Beer–Lambert law, the concentration of MB is proportional to the absorbance of MB, and then the degradation efficiency of MB can be calculated by[49, 50].

$$R = \frac{C_0 - C_t}{C_0} \times 100\% = \frac{A_0 - A_t}{A_0} \times 100\% \quad (1)$$

Where C_0 , C_t and A_0 , A_t are the concentration and absorbance of MB at $t=0$ and $t=t$ reaction time. Since the photocatalytic reaction rate depends on the concentration of the organic pollutants, we adopted the method developed by Xu et al. for MB degradation on TiO_2 where he proposes that the MB degradation obeys a pseudo-first-order kinetics law[51].

Using a plot of MB concentration (C_t) as a function of irradiation time and we will describe the degradation of MB by a pseudo-first-order kinetics as given by the following equation (Eq. (2))[44]:

$$-\frac{dC_t}{dt} = k_{app} \times t \quad (2)$$

Where C_t is the concentration of MB for time t and k_{app} is the apparent MB degradation rate constant. By integration and using with the boundary conditions $C_t = C_0$ for $t=0$ and $C_t = C_t$ for $t=t$, the results will lead to Eq. (3):

$$\ln\left(\frac{C_0}{C_t}\right) = k_{app} \times t \quad (3)$$

All k_{app} values were calculated for a same initial concentration of MB (5 mg/L) and at various Ag/ZnO doses. Figure 5 show the photodegradation curves of MB in the form of $\ln\left(\frac{C_0}{C_t}\right)$ versus time and the determined values of reaction rate constant k_{app} , from linear fitting of each dose.

The degradation efficiencies of Ag/ZnO photocatalyst are investigated. Table 1 present the MB degradation rate constant k_{app} and the ratio between k_{app} (min^{-1})-UV and k_{app} (min^{-1})-Visible of Ag/ZnO photocatalysts as a function of Ag/ZnO photocatalyst dose. These results agree with the results obtained by Ahmed A. Abdel-Khalek et al. for the photodegradation of Methylene green (MG) and attributed the increase in the photodegradation rate to the increase in the catalyst concentration which increases the number of active sites on catalyst surface which lead to increase in the number of $\text{OH}\cdot$ and $\text{OH}_2\cdot$ radicals[52].

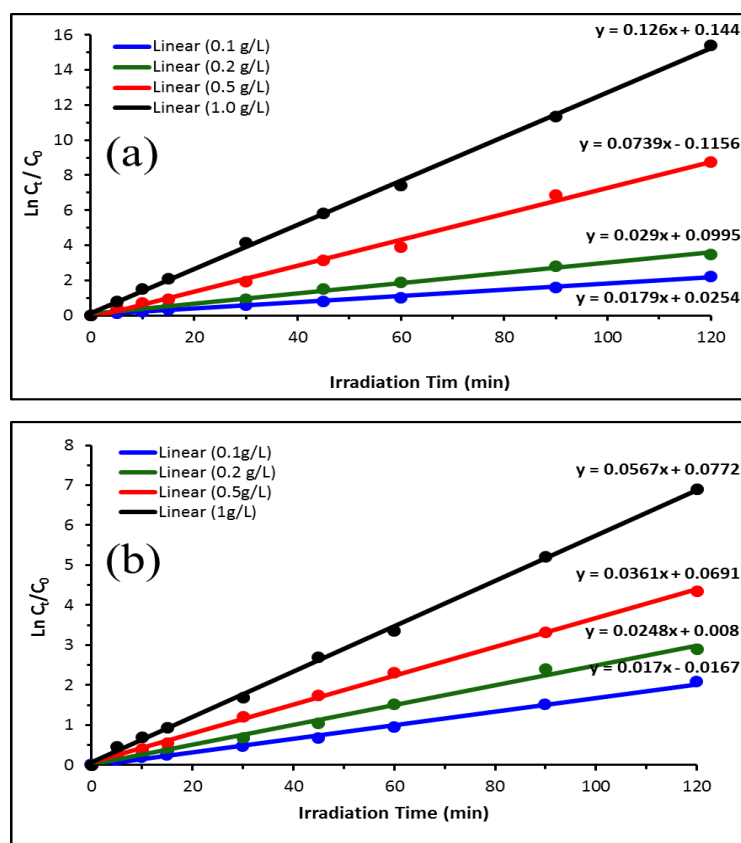


Figure 7: Kinetic study and Pseudo-first order fitting of the kinetics of MB removal during photocatalytic degradation of MB using different doses of Ag/ZnO Photocatalyst. A) UV light. B) Visible Light. Reaction conditions: UV (UV-L (254 nm), 15 w) and visible light irradiation: 1000 W, 5 mg/L MB, natural pH 5.8, room temperature (23-25 °C).

Table 1 summarised the MB degradation rate constant k_{app} and the ratio between $k_{app}(\text{min}^{-1})\text{-UV} / k_{app}(\text{min}^{-1})\text{-Visible}$ of Ag/ZnO photocatalysts as a function of Ag/ZnO photocatalyst dose.

| Ag/ZnO-UV (g/L) | $k_{app}(\text{min}^{-1})\text{-UV}$ | $k_{app}(\text{min}^{-1})\text{-Visible (g/L)}$ | Ratio $k_{app}(\text{min}^{-1})\text{-UV} / k_{app}(\text{min}^{-1})\text{-Visible}$ |
|-----------------|--------------------------------------|---|--|
| 0.1 | 0.0179 | 0.0170 | 1.05 |
| 0.2 | 0.029 | 0.0248 | 1.17 |
| 0.5 | 0.0739 | 0.0361 | 2.05 |
| 1 | 0.126 | 0.0567 | 2.22 |

The k_{app} values vs. catalyst dose suggest that MB degradation rate under UV or visible light irradiation increases linearly with the increase of catalyst dose. These results were reported by L.-Y. Yang et al.[6] which suggest that the photocatalytic degradation kinetics of MB fitted the pseudo-first-order kinetics and the Langmuir–Hinshelwood model (L-H)[53]. Finally, using Pseudo-first order fitting of the kinetics of MB removal during photocatalytic degradation of MB under UV or visible light irradiation, the rate constant (k_{app}) of the MB degradation can be estimated.

Figure 8 shows a comparison of apparent MB degradation rate constant k_{app} as a function of Ag/ZnO photocatalyst concentration under UV and Visible light irradiation.

Our results showed that the MB degradation rate constant for Ag/ZnO photocatalyst under UV light is 0.124 min^{-1} which is 16 times faster than ZnO photocatalyst (0.008 min^{-1}) and the MB degradation rate constant for Ag/ZnO photocatalyst under Visible light is 0.043 min^{-1} which is 5 times faster than ZnO photocatalyst (0.008 min^{-1}) [41]. While the MB degradation rate constant under UV light, is three times faster than the MB degradation rate constant under visible light with the same conditions. MB photocatalytic degradation experiments proved that synthesised samples of Ag/ZnO nanoparticles have excellent activity toward

decomposition of MB under UV and visible light irradiation which follow the 1st order kinetic mechanism. The MB was successfully removed from water by the photocatalytic oxidation reaction under the UV and Visible irradiation conditions. Similar results reported by Patil et al. using the sun simulated light[54].

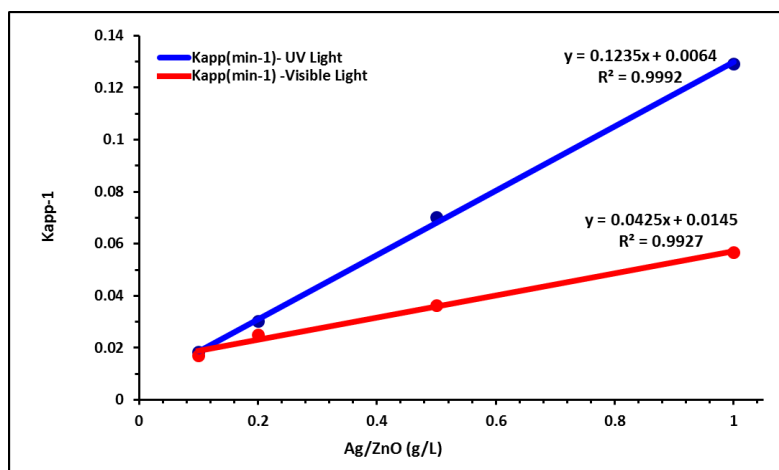


Figure 8: Comparison of apparent MB degradation rate constant k_{app} as a function of Ag/ZnO photocatalyst concentration under UV and Visible light irradiation. All k_{app} values were calculated for a same initial concentration of MB (5 mg/L) and at various Ag/ZnO doses. The profile of k_{app} values vs. Ag/ZnO dose suggests that MB degradation rate by UV and Visible light irradiation process increases linearly with the increase of Ag/ZnO dose.

We attributed the enhanced photocatalytic activity to the interaction between Ag metal nanospheres and ZnO nanorods, where effective electron transfer leads to the reduction of electron/hole pairs recombination which is mainly due to the decrease of energy band gap in Ag/ZnO nanocomposites and the formation of Schottky barriers in the regions between Ag nanospheres and ZnO nanorods in the case of UV light irradiation and the strong localized Surface Plasmon Resonance (SPR) in the case of visible light irradiation.

3.3 MB degradation mechanism on Ag/ZnO under UV and Visible Light Irradiation

Based on our results, we can propose an MB photodegradation reaction mechanism based on the mechanism proposed recently by many researchers. S. Mohammad Zadeh et al.[55, 56] proposed a mechanism for the photodegradation of dyes on the Ag/ZnO photocatalyst based on the work function of ZnO (5.2 eV) and Ag (4.26 eV) where the Fermi energy level of Ag is higher than the Fermi level of ZnO. The electrons are transferred from the Fermi level of Ag to the Fermi level of ZnO due to the larger work function of ZnO. The equilibrium of the two Fermi levels leads to the formation of new Fermi energy level for Ag/ZnO, as reported by Saravanan et al.[57]. In this model, the UV irradiation excites the electrons from the valence band of ZnO to the conduction band and leaves the corresponding holes in the valence band. Then the photoexcited electrons are transferred to Ag since the conduction band of ZnO is at higher energy than Fermi energy level for Ag/ZnO as reported by Pyne et al. [58]. As a result, the electron-hole separation efficiency is enhanced. This leads to the photocatalytic oxidation of the dye through the reaction of the holes in the valence band of ZnO with water and hydroxyl groups to form $\text{OH}\cdot$ radicals and in parallel, the photogenerated electrons react with O_2 to form active oxygen species, which also lead to the photocatalytic oxidation of the dye as reported by many researchers.[59, 60]. However, the mechanism for the photodegradation of dyes on the Ag/ZnO photocatalyst under visible light (or sunlight) is slightly different. The mechanism for visible light driven photodegradation is based on the direct electron transfer from semiconductor surface to the plasmonic nanostructures and is strongly dependent on the alignment of the electronic band structure of the noble metal and semiconductor[55]. In these mechanisms, the enhanced photocatalytic degradation of MB activity on Ag/ZnO photocatalyst can be explained by the plasmonic effect or Surface Plasmon Resonance (SPR) of Ag nanoparticles where the Ag nanoparticles extend the light absorption range of ZnO from near UV to the visible light region, which leads to enhancement of absorption efficiency. Also, Ag nanoparticles can further enhance the charge separation in ZnO by absorbing more photons with energy greater than or equal to ZnO band gap, where more electrons are promoted from valence band to conduction band, creating corresponding holes in the valence band followed by the electron transfer from ZnO to Ag nanoparticles, since the energy level of conduction band of ZnO is at higher energy level than the Fermi level of Ag/ZnO nanocomposites as mentioned above. As a result, Ag nanoparticles act as a

sink for photo-generated electrons and play a paramount role in preventing electron-hole recombination with holes[61]. Upon irradiation with visible light, the MB dye molecules are excited and adsorbed onto the ZnO nanoparticles and then transfer electrons into the conduction band of ZnO[62]. Then the photodegradation of MB proceeds according to the process mentioned above. The effect of Ag on enhancing the photocatalytic activity could be explained by its ability to trap electrons, which decreases recombination of electrons on Ag and holes on the ZnO by producing more $\text{OH}\cdot$ [63].

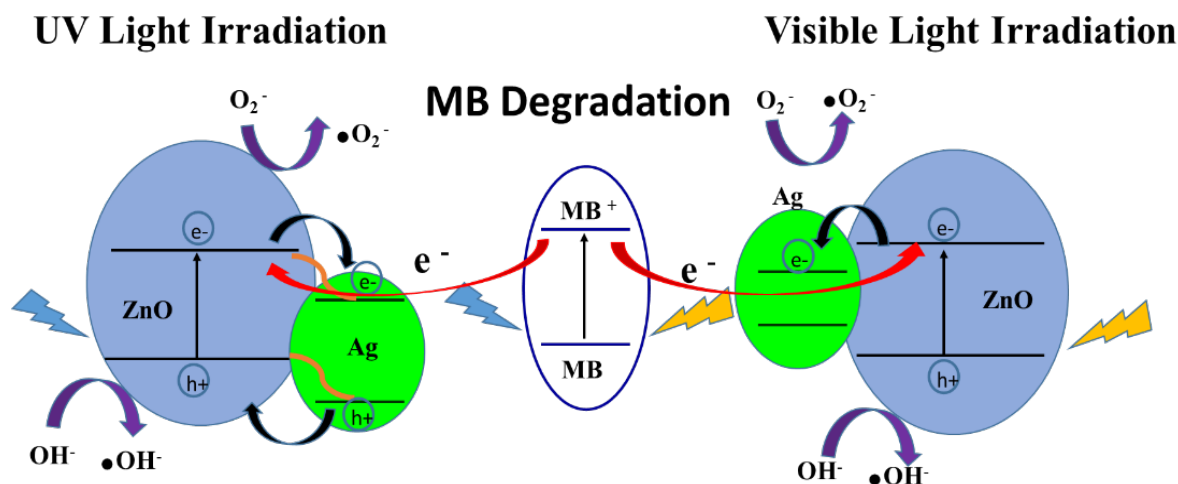


Figure 9: MB photodegradation reaction mechanism on Ag/ZnO under UV and visible light irradiation.

4. Anti-Bacterial Activity of ZnO and Ag/ZnO Nanocomposites

ZnO nanorods have been used for water treatment and known for their ability to degrade organic dyes such as methylene blue and methyl orange, as well as the inactivation of both Gram negative and Gram positive of bacteria like *Escherichia coli*, *Bacillus subtilis*, and *Staphylococcus aureus*[64-66]. Baruah et al. attribute higher degradation rates to the higher active surface area of nanorods arrays[48]. Antibacterial activity of ZnO and Ag/ZnO nanorods was reported by many researchers[67-69]. The improved bioactivities of Ag/ZnO nanocomposites were enhanced due to the presence of the silver ion and the higher surface to volume ratio. The silver ions are well known to have high toxicity toward different types of microorganisms including *E. coli* [27, 40, 70]. Subhan et al. attributed the high antibacterial activity of Ag/ZnO nanorods to the small size and the large surface area which generate more active oxygen species to cover the bacterial colony and increase the mechanical damage the bacteria cells, and eventually kill bacteria more efficiently[63].

In this study, the antibacterial activity of ZnO and Ag/ZnO towards Gram-negative (*E. coli*) bacteria culture was studied under a controlled environment. The test was performed based as follow: a filter paper was cut into small squares (about 0.5 cm across) to accommodate the Zinc Oxide (ZnO), Silver on Zinc oxide (Ag-ZnO) and all needed controls (broth & non-soaked filter paper). Then, the filter paper squares are placed in Petri dishes and pour the test tube of nanoparticles over the squares while preparing the controls needed in the other Petri dishes. The filter paper squares are left to soak for 10 minutes (or longer). The bottom of an agar plate is marked and divided into sections to accommodate the silver-soaked filter and all controls, and label each section. Then, a 20 mL of bacterial culture are placed on the agar plate using a disposable transfer pipet, and the drops of bacteria culture are spread on the agar plate using a cotton swab. Finally, the nanoparticles-soaked filter paper squares and control(s) are kept in a designated areas followed by incubating agar plate for 24 hours at 37°C. The agar plate monitored and examined every day by taking their picture and recording notes. The inhibition zone around the filter indicates the antibacterial effect of Ag-ZnO nanocomposites.

The antibacterial activity of the samples and the controls were evaluated under visible light and in the dark for seven months. Anti-bacterial test of both samples under visible light shows no evidence of bacterial colonies growth around the filter as shown in the figure. 9. While a bacterial colonies growth is shown on the control filter.

On the other hand, the anti-bacteria activity of the samples and the control in the dark shows that there is no evidence of bacteria colonies growth of ZnO-coated filter after the first 72 hours; then the bacterial colonies grew after five days. These results indicate the deactivation of ZnO photocatalyst due to the recombination of electro-hole pairs in ZnO as shown in figure 10.

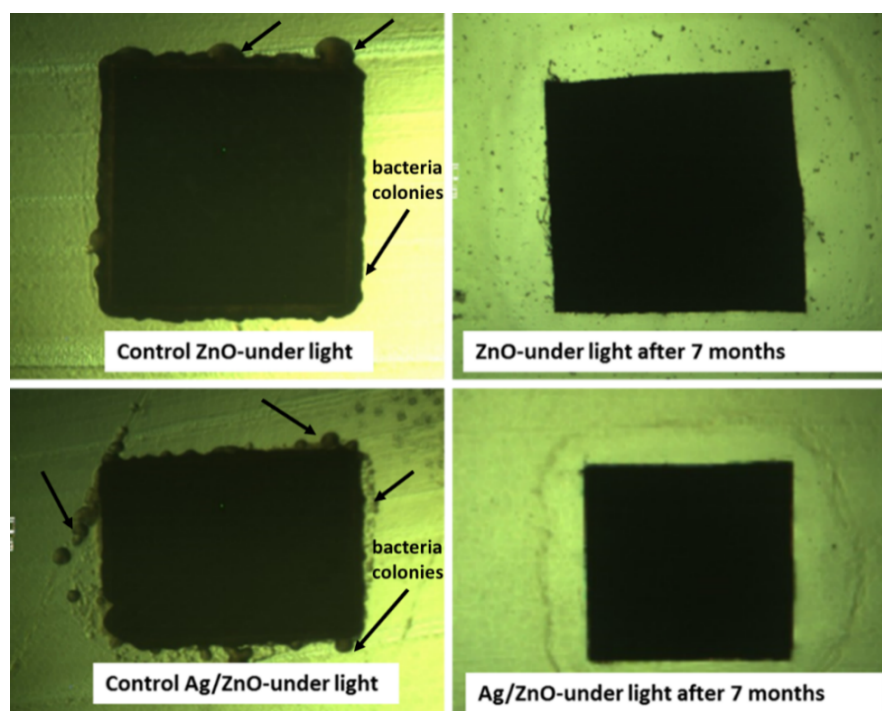


Figure 10: Photograph of a filter paper with and without ZnO and Ag/ZnO nanocomposites. Dark spots are bacteria colonies.

However, in the case of Ag/ZnO nanocomposites, the anti-bacteria activity shows no evidence of bacteria colonies growth even after seven months as shown in figure 11. These results can be attributed to the presence of the silver ions which are known to have anti-bacterial activity when they come in contact with the bacteria.

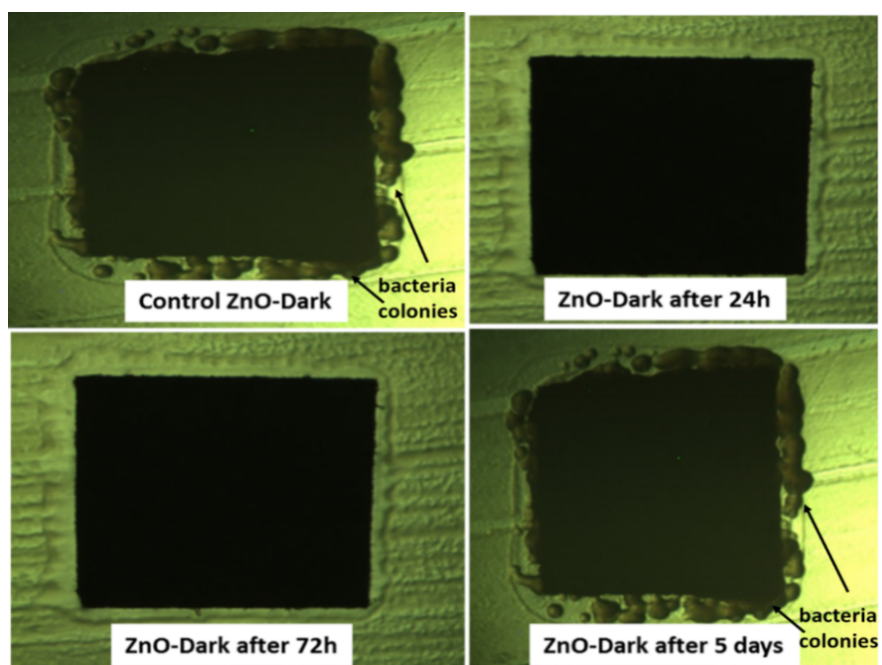


Figure 11: Photograph of a filter paper with ZnONanorods after five days. Dark spots are bacterial colonies.

We observed enhanced antibacterial activity of ZnO and Ag/ZnO nanocomposites towards Gram-negative Escherichia coli (E. coli) bacteria culture under visible light illumination and in dark conditions compared to the control. We monitor the bioactivities of ZnO and Ag/ZnO nanocomposites for seven months. Both photocatalysts show high antibacterial activities (no bacterial culture growth) under visible light

illumination. However, under dark conditions, ZnONanorods has small inactivation efficiency of Gram-negative (*E. coli*) after almost two days and this evident by bacterial culture growth in the inhibition zone. In the case of Ag/ZnONanorods, the inactivation efficiencies were high and no evidence of growth. The improved antibacterial activities of Ag/ZnO photocatalyst can be attributed to small particles size, higher surface to volume ratio, which can cover the bacterial colony, and the results in the generation of active oxygen species on the surface of the photocatalyst and hence will kill bacteria more effectively[67].

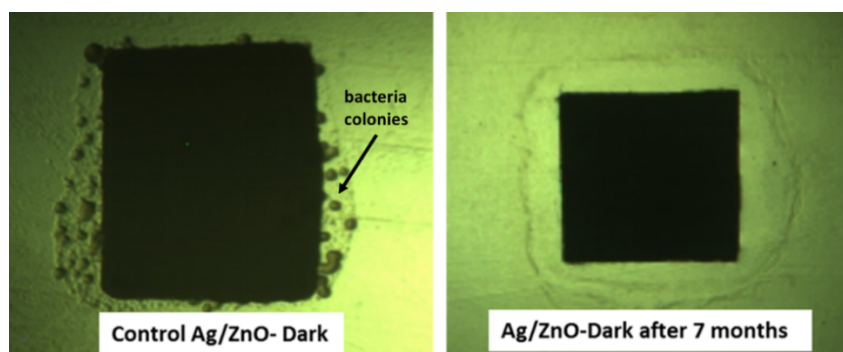


Figure 12: Photograph of a filter paper with Ag/ZnO Nanocomposite after seven months. Dark spots are bacteria colonies.

Our results agreed perfectly with the results reported by Vora et al. where significant bacterial cell membrane damage and DNA degradation was observed following the visible light illumination[54]. Also, Baruah et al. report the inactivation efficiencies of ZnONanorods under bright conditions and dark conditions and found that the inactivation efficiencies are doubled compared to the dark conditions. They found that cell membrane damaged and DNA degradation was observed only under illumination due to photocatalytic electron injection process, while inactivation in the dark is primarily attributable to the bactericidal effect of Zn^{2+} ions [59].

Conclusion

The present study shows a systematic overview and comparison between the catalytic activity and antibacterial properties of ZnO and Ag/ZnO composites under different irradiation conditions. The differences between the photocatalytic efficiencies and the antibacterial properties were correlated with the shift of the material's optical, photocatalytic and the structural properties as a result of the presence of the silver. It was shown that the photocatalytic degradation of MB using bare ZnONanorods was increased significantly with faster rate compared to the control (UV light only). Upon incorporating the silver to the ZnONanorods, the rate of MB degradation proceeds faster. The degradation rate constant was found of being three times higher under UV light irradiation than visible light irradiation and 16 times greater when compared the rate of ZnONanorods under similar conditions and can be fitted into pseudo-first-order kinetics and the Langmuir–Hinshelwood model.

Furthermore, the antibacterial activity of ZnO and Ag/ZnO nanocomposites towards Gram-negative *Escherichia coli* (*E. coli*) bacteria culture under visible light illumination and in dark conditions is studied and is compared with the control. The bioactivities of ZnO and Ag/ZnO nanocomposites monitored for seven months. Both photocatalysts show high antibacterial activities (no bacterial culture growth) under visible light illumination. However, under dark conditions, ZnONanorods have no inactivation efficiency of Gram-negative (*E. coli*) after almost two days while Ag/ZnONanorods have high inactivation efficiencies and no evidence of growth after seven months.

We attribute the enhanced photocatalytic and antibacterial activities of Ag/ZnO nanoparticles to the synergetic effect and Surface Plasmon effect of Ag nanoparticles along with improved charge transfer, and the prevention of the electro-hole recombination in ZnO. Also, the presence of the silver, serve as an electron sink and prevent electron-hole recombination and enhance the absorption in the UV and the visible solar radiation due to the plasmonic effect and at the same time increase the inactivation efficiency of Gram-negative (*E. coli*).

Acknowledgments-The authors are pleased to acknowledge Virginia Commonwealth university in Qatar (VCU Qatar) for providing the facilities for the research. Also the Director of Liberal Arts and Science Program Patty Paine, Dean of VCU Qatar Dr. AkelKahera for their continuous support.

References

1. S. Baruah, J. Dutta, *Environ Chem. Lett.* 7 (2009) 191-204.
2. M.R. Hoffmann, S.T. Martin, W. Choi, D.W. Bahnemann, *Chem. Rev.* 95 (1995) 69-96.
3. P. Periyat, S.C. Pillai, D.E. McCormack, J. Colreavy, S.J. Hinder, *The J. Phys. Chem. C* 112 (2008) 7644-7652.
4. M.E. Simonsen, *Heterogeneous Photocatalysis, Chemistry of Advanced Environmental Purification Processes of Water*, Elsevier, 2014, pp. 135-170.
5. G. Merga, L.C. Cass, D.M. Chipman, D. Meisel, *J. Am. Chem. Soc.* 130 (2008) 7067-7076.
6. L.-Y. Yang, S.-Y. Dong, J.-H. Sun, J.-L. Feng, Q.-H. Wu, S.-P. Sun, *J. Hazard. Mater.* 179 (2010) 438-443.
7. C.A.K. Gouvêa, F. Wypych, S.G. Moraes, N. Durán, N. Nagata, P. Peralta-Zamora, *Chemosphere* 40 (2000) 433-440.
8. A. Errekato, A. Ibarra, A. Gutierrez, J. Bilbao, J.M. Arandes, P. Castano, *Chem. Eng. J.* 307 (2017) 955-965.
9. R.A.M. Esfahani, L. Osmieri, S. Specchia, S. Yusup, A. Tavasoli, A. Zamaniyan, *Chem. Eng. J.* 308 (2017) 578-587.
10. A.B. Fadhil, A.I. Ahmed, H.A. Salih, *Fuel* 187 (2017) 435-445.
11. B. Dindar, S. Içli, *J. Photochem. Photobiol. A: Chemistry* 140 (2001) 263-268.
12. Ö.A. Yıldırım, H.E. Unalan, C. Durucan, *J. Am. Ceram. Soc.* 96 (2013) 766-773.
13. Y. Liu, S. Wei, W. Gao, *J. Hazard. Mater.* 287 (2015) 59-68.
14. T.Y. Liu, W. Chen, Y.X. Hua, X.H. Liu, *Appl. Surf. Sci.* 392 (2017) 616-623.
15. A. Alzahrani, D. Barbash, A. Samokhvalov, *J. Phys. Chem. C* 120 (2016) 19970-19979.
16. S.C. Padmanabhan, S.C. Pillai, J. Colreavy, S. Balakrishnan, D.E. McCormack, T.S. Perova, S.J. Hinder, J.M. Kelly, *Chem. Mater.* 19 (2007) 4474-4481.
17. P.V. Kamat, *The Journal of Phys. Chem. B* 106 (2002) 7729-7744.
18. L. Cai, F. Ren, M. Wang, G.X. Cai, Y.B. Chen, Y.C. Liu, S.H. Shen, L.J. Guo, *Int. J. Hydrog. Energy* 40 (2015) 1394-1401.
19. E. Stathatos, T. Petrova, P. Lianos, *Langmuir* 17 (2001) 5025-5030.
20. X. Liu, W. Li, N. Chen, X. Xing, C. Dong, Y. Wang, *RSC Adv.* 5 (2015) 34456-34465.
21. P. Fageria, S. Gangopadhyay, S. Pande, *RSC Adv.* 4 (2014) 24962-24972.
22. X. Chen, H.J. Schluesener, *Toxicol Lett* 176 (2008) 1-12.
23. P. Rauwel, E. Rauwel, S. Ferdov, M.P. Singh, *Adv. Mater. Sci. Eng.* 2015 (2015) 1-2.
24. A. Haider, I.-K. Kang, *Adv. Mater. Sci. Eng.* 2015 (2015) 1-16.
25. R. Vaidyanathan, K. Kalishwaralal, S. Gopalram, S. Gurunathan, *Biotechnol. Adv.* 27 (2009) 924-937.
26. R. Vaidyanathan, K. Kalishwaralal, S. Gopalram, S. Gurunathan, *Biotechnol. Adv.* 28 (2010) 940.
27. J.A. Spadaro, T.J. Berger, S.D. Barranco, S.E. Chapin, R.O. Becker, *Antimicrob. Agents Chemother.* 6 (1974) 637-642.
28. L.P. Miller, S.E.A. McCallan, *J. Agric. Food. Chem.* 5 (1957) 116-122.
29. J.S. Kim, E. Kuk, K.N. Yu, J.-H. Kim, S.J. Park, H.J. Lee, S.H. Kim, Y.K. Park, Y.H. Park, C.-Y. Hwang, Y.-K. Kim, Y.-S. Lee, D.H. Jeong, M.-H. Cho, *Nanomed. Nanotechnol. Biol. Med.* 3 (2007) 95-101.
30. H.R. Pant, B. Pant, R.K. Sharma, A. Amarjargal, H.J. Kim, C.H. Park, L.D. Tijing, C.S. Kim, *Ceram. Int.* 39 (2013) 1503-1510.
31. S. Paul, S. Ghosh, M. Saha, S.K. De, *Phys. Chem. Chem. Phys.* 18 (2016) 13092-13107.
32. Y.H. Lu, M. Xu, L.X. Xu, C.L. Zhang, Q.P. Zhang, X.N. Xu, S. Xu, K. Ostrikov, *J. Nanopart. Res.* 17 (2015).
33. K.I. Milenova, K.L. Zaharieva, I.D. Stambolova, V.N. Blaskov, A.E. Eliyas, *BulgChem. Commun.* 49 (2017) 95-99.
34. M. Moradi, M. Haghighi, S. Allahyari, *Process Saf. Environ. Prot.* 107 (2017) 414-427.
35. S. Naghizadeh-Alamdari, A. Habibi-Yangjeh, M. Pirhashemi, *Solid State Sci.* 40 (2015) 111-120.
36. B.M. Rajbongshi, A. Ramchiary, B.M. Jha, S.K. Samdarshi, *J. Mater. Sci. - Mater. Electron.* 25 (2014) 2969-2973.
37. M.J. Sampaio, M.J. Lima, D.L. Baptista, A.M.T. Silva, C.G. Silva, J.L. Faria, *Chem. Eng. J.* 318 (2017) 95-102.
38. S.T. Tan, A.A. Umar, A. Balouch, S. Nafisah, M. Yahaya, C.C. Yap, M.M. Salleh, I.V. Kityk, M. Oyama, *Acs Comb. Sci.* 16 (2014) 314-320.
39. H.F. Wang, X.Q. Liu, S. Han, *Cryst. Eng. Comm.* 18 (2016) 1933-1943.
40. X.H. Zhao, S. Su, G.L. Wu, C.Z. Li, Z. Qin, X.D. Lou, J.G. Zhou, *Appl. Surf. Sci.* 406 (2017) 254-264.
41. K. Saoud, R. Alsoubaihi, N. Bensalah, T. Bora, M. Bertino, J. Dutta, *Mater. Res. Bull.* 63 (2015) 134-140.

42. N. Zhuo, L. Li, Y. Gao, L. Lu, X.D. Huang, L.L. Wang, *Chin.J. Inorg. Chem.* 29 (2013) 991-998.
43. T. Huang, X.-H.N. Xu, *J. Mater. Chem.* 20 (2010) 9867.
44. S. Sarkar, D. Basak, *Cryst.Eng. Comm.* 15 (2013) 7606.
45. Y. Gong, Y. Zhou, L. He, B. Xie, F. Song, M. Han, G. Wang, *The Eur. Phys. J. D* 67 (2013).
46. D. Zhang, X. Pu, H. Li, Y.M. Yu, J.J. Shim, P. Cai, S.I. Kim, H.J. Seo, *Mater. Res. Bull.* 61 (2015) 321-325.
47. H. Liu, Y. Hu, Z. Zhang, X. Liu, H. Jia, B. Xu, *Appl. Surf. Sci.* 355 (2015) 644-652.
48. S. Baruah, S. K. Pal, J. Dutta, *J. Nanosci. Nanotechnol. Asia* 2 (2012) 90-102.
49. K. Wang, L. Yu, S. Yin, H. Li, H. Li, *Pure Appl. Chem.* 81 (2009).
50. Y. Abdollahi, A.H. Abdullah, Z. Zainal, N.A. Yusof, *Int. J. Mol. Sci.* 13 (2011) 302-315.
51. N. Xu, Z. Shi, Y. Fan, J. Dong, J. Shi, M.Z.C. Hu, *Ind. Eng. Chem. Res.* 38 (1999) 373-379.
52. A.A. Abdel-Khalek, H.F. Nassar, F.K. Abdel-Gawad, S.M. Basem, S. Awad, *Quantum Matter* 5 (2016) 297-304.
53. J.J. Vora, S.K. Chauhan, K.C. Parmar, S.B. Vasava, S. Sharma, L.S. Bhutadiya, *E-J. Chem.* 6 (2009) 531-536.
54. S.S. Patil, M.G. Mali, M.S. Tamboli, D.R. Patil, M.V. Kulkarni, H. Yoon, H. Kim, S.S. Al-Deyab, S.S. Yoon, S.S. Kolekar, B.B. Kale, *Catal. Today* 260 (2016) 126-134.
55. M. Farbod, M. Khademalrasool, M.D. Talebzadeh, *Plasmonics* 12 (2017) 759-769.
56. S. Mohammadzadeh, M.E. Olya, A.M. Arabi, A. Shariati, M.R. Khosravi Nikou, *J. Environ. Sci.* 35 (2015) 194-207.
57. R. Saravanan, N. Karthikeyan, V.K. Gupta, E. Thirumal, P. Thangadurai, V. Narayanan, A. Stephen, *Mater. Sci. Eng. C* 33 (2013) 2235-2244.
58. S. Pyne, G.P. Sahoo, D.K. Bhui, H. Bar, P. Sarkar, S. Samanta, A. Maity, A. Misra, *Spectrochim. Acta, Part A* 93 (2012) 100-105.
59. Y. Cai, H. Fan, M. Xu, Q. Li, *Colloids Surf., A* 436 (2013) 787-795.
60. C. Ren, B. Yang, M. Wu, J. Xu, Z. Fu, Y. Lv, T. Guo, Y. Zhao, C. Zhu, *J. Hazard. Mater.* 182 (2010) 123-129.
61. S. Kuriakose, V. Choudhary, B. Satpati, S. Mohapatra, *Phys. Chem. Chem. Phys.* 16 (2014) 17560.
62. S. Rehman, R. Ullah, A.M. Butt, N.D. Gohar, *J. Hazard. Mater.* 170 (2009) 560-569.
63. S. Sakthivel, B. Neppolian, M.V. Shankar, B. Arabindoo, M. Palanichamy, V. Murugesan, *Sol. Energy Mater. Sol. Cells* 77 (2003) 65-82.
64. A. Sapkota, A.J. Anceno, S. Baruah, O.V. Shipin, J. Dutta, *Nanotechnology* 22 (2011) 215703.
65. S. Baruah, M. Jaisai, R. Imani, M.M. Nazhad, J. Dutta, *Sci. Technol. Adv. Mater.* 11 (2010) 055002.
66. S. Baruah, M. Najam Khan, J. Dutta, *Environ. Chem. Lett.* 14 (2015) 1-14.
67. S. H, Manikandan, B. Ahmed M, G. V, *J. Nanomed. Nanotechnol.* 04 (2017).
68. I. Matai, A. Sachdev, P. Dubey, S. Uday Kumar, B. Bhushan, P. Gopinath, *Colloids Surf., B* 115 (2014) 359-367.
69. M.A. Subhan, M.R. Awal, T. Ahmed, M. Younus, *Acta Metall. Sinica -Eng. Lett.* 27 (2014) 223-232.
70. G. Zhao, J.S.E. Stevens, *Biometals* 11 (1998) 27-32.

(2018) ; <http://www.jmaterenvironsci.com>